Appl Compos Mater (2009) 16:379–392
DOI 10.1007/s10443-009-9105-7

Effects of Steam Environment on Creep Behavior of Nextel™610/Monazite/Alumina Composite at 1,100°C

Marina B. Ruggles-Wrenn · Tufan Yeleser · Geoff E. Fair · Janet B. Davis

Received: 3 August 2009 / Accepted: 24 September 2009 / Published online: 14 October 2009

Abstract The tensile creep behavior of a N610™/$LaPO_4$/Al_2O_3 composite was investigated at 1,100°C in laboratory air and in steam. The composite consists of a porous alumina matrix reinforced with Nextel 610 fibers woven in an eight-harness satin weave fabric and coated with monazite. The tensile stress-strain behavior was investigated and the tensile properties measured at 1,100°C. The addition of monazite coating resulted in ~33% improvement in ultimate tensile strength (UTS) at 1,100°C. Tensile creep behavior was examined for creep stresses in the 32–72 MPa range. Primary and secondary creep regimes were observed in all tests. Minimum creep rate was reached in all tests. In air, creep strains remained below 0.8% and creep strain rates approached 2×10^{-8} s^{-1}. Creep run-out defined as 100 h at creep stress was achieved in all tests conducted in air. The presence of steam accelerated creep rates and significantly reduced creep lifetimes. In steam, creep strain reached 2.25%, and creep strain rate approached 2.6×10^{-6} s^{-1}. In steam, creep run-out was not achieved. The retained strength and modulus of all specimens that achieved run-out were characterized. Comparison with results obtained for N610™/Al_2O_3 (control) specimens revealed that the use of the monazite coating resulted in considerable improvement in creep resistance at 1,100°C both in air and in steam. Composite microstructure, as well as damage and failure mechanisms were investigated.

Keywords Ceramic-matrix composites (CMCs) · Fibers · Coatings · Creep · High-temperature properties

The views expressed are those of the authors and do not reflect the official policy or position of the United States Air Force, Department of Defense or the U. S. Government.

M. B. Ruggles-Wrenn (✉) · T. Yeleser
Aeronautics & Astronautics, Air Force Institute of Technology, Wright-Patterson Air Force Base, OH 45433-7765, USA
e-mail: marina.ruggles-wrenn@afit.edu

G. E. Fair
Materials and Manufacturing Directorate, Air Force Institute of Technology, Wright-Patterson Air Force Base, OH 45433-7817, USA

J. B. Davis
Teledyne Scientific, Thousand Oaks, CA 91360, USA

1 Introduction

Advances in power generation systems for aircraft engines, land-based turbines, rockets, and, most recently, hypersonic missiles and flight vehicles have raised the demand for structural materials that have superior long-term mechanical properties and retained properties under high temperature, high pressure, and varying environmental factors, such as moisture [1]. Typical components include combustors, nozzles and thermal insulation. Ceramic-matrix composites (CMCs), capable of maintaining excellent strength and fracture toughness at high temperatures are prime candidate materials for such applications. Additionally, lower densities of CMCs and their higher use temperatures, together with a reduced need for cooling air, allow for improved high-temperature performance when compared to conventional nickel-based superalloys [2]. Advanced reusable space launch vehicles will likely incorporate fiber-reinforced CMCs in critical propulsion components [3]. Because these applications require exposure to oxidizing environments, the thermodynamic stability and oxidation resistance of CMCs are vital issues. The need for environmentally stable composites motivated the development of CMCs based on environmentally stable oxide constituents [4–9].

The main advantage of CMCs over monolithic ceramics is their superior toughness, tolerance to the presence of cracks and defects, and non-catastrophic mode of failure. It is widely accepted that in order to avoid brittle fracture behavior in CMCs and improve the damage tolerance, a weak fiber/matrix interface is needed, which serves to deflect matrix cracks and to allow subsequent fiber pullout [10–12]. It has been demonstrated that similar crack-deflecting behavior can also be achieved by means of a finely distributed porosity in the matrix instead of a separate interface between matrix and fibers [13]. Resulting oxide/oxide CMCs exhibit damage tolerance combined with inherent oxidation resistance. In this case, there is a strong bonding between the fiber and matrix; consequently, a minimum matrix porosity is needed for this concept to work [14]. An extensive review of the mechanisms and mechanical properties of porous-matrix CMCs is given in [1,15].

For a dense (>90%) matrix composite, an interfacial coating is needed for crack deflection. An extensive review of the research on oxide coatings for oxide and non-oxide composites has been given by Kerans et al. [12]. The development of oxide-oxide composites that rely on a weak fiber/matrix interface for crack deflection prompted research into oxidation resistant fiber coatings that are chemically stable with the composite constituents. Monazite ($LaPO_4$) is among the various oxidation-resistant coating materials that have been investigated. Several studies showed [16–19] that due to the chemical compatibility of monazite with alumina at high temperature, monazite was a good candidate for a weak interface material for alumina-based composites. Since then, multiple investigations into the production of monazite coatings and its use with different fiber/matrix combinations [20–22] have been carried out. Hay [23] and Boakye et al. [24] developed a process for coating continuous fiber tows with monazite that utilizes washed sols. More recently, Fair et al. [25, 26] developed a method for coating woven cloths of ceramic fibers with monazite using precipitation from solution precursors.

Porous-matrix oxide/oxide CMCs exhibit several behavior trends that are distinctly different from those exhibited by traditional CMCs with a fiber-matrix interface. Most SiC-fiber-containing CMCs exhibit longer life under static loading and shorter life under cyclic loading [27]. For these materials, fatigue is significantly more damaging than creep. Conversely, for porous-matrix oxide-oxide CMCs, creep is considerably more damaging than fatigue [28, 29]. In addition, the prior studies [29, 30] revealed that creep performance of the porous-matrix Nextel™720/alumina (N720/A) oxide-oxide composite deteriorates

drastically in the presence of steam. Due to these findings, high-temperature creep resistance remains among the key issues that must be addressed before using oxide-oxide CMCs in advanced aerospace applications. The objective of this study is to investigate the effects of monazite fiber coating on creep resistance of Nextel™610/alumina (N610/A) composite at 1,100°C in air and in steam. Keller et al. [31] investigated the effectiveness of monazite coatings in Nextel™610/alumina porous-matrix composites after long-term exposure at 1,100°C and 1,200°C. Coated fiber samples exhibited better tensile strength retention after 1,000 h at 1,200°C when compared to the control (uncoated fiber) material. Ruggles-Wrenn et al. [32] reported that the use of monazite coating improved the creep resistance at 900°C of the N610/A porous-matrix CMC consisting of unidirectional plies in a symmetric cross-ply orientation of $[(0°/90°)]_{2S}$. The present effort aims to evaluate the creep behavior of the Nextel™610/monazite/alumina (N610/M/A) composite comprised of eight 0°/90° woven layers. Creep tests were conducted at 1,100°C in air and in steam for stress levels ranging from 32 MPa to 72 MPa. Resulting creep performance imposes limitations on the use of these materials in high-temperature applications. The composite microstructure, as well as damage and failure mechanisms are discussed.

2 Material and Experimental Arrangements

The material studied was Nextel™610/monazite/alumina (N610/M/A), an oxide-oxide ceramic composite composed of Nextel™610 fibers coated with monazite and an alumina matrix. Cloths of Nextel™610 fibers woven in an eight harness satin weave (8HSW) were coated with monazite by precipitation process developed by Fair et al. [25, 26]. Five coats were applied to the cloths using citric acid precursors with intercoat firings at 600°C. Coated cloths were given a final firing at 1,200°C for 2 h prior to composite manufacture.

The alumina matrices were produced by pressure filtration using a large stainless steel pressure vessel with a porous sintered stainless steel filter to allow liquid drainage. Eight woven cloth layers were stacked on the porous steel filter for composite processing. The alumina powder slurry was placed in a reservoir with a volume of approximately 2 L. Throughout the infiltration process the alumina powder slurry, which was stirred constantly was pumped into the vessel using a peristaltic pump. The alumina slurry contained approximately 5-volume percent of 150 nm alumina powder (TM-DAR, Taimei Chemicals) dispersed at pH 4. Because of the low solids content of the slurry and limited size of the reservoir, the vessel had to be refilled several times to build up the matrix through the entire thickness of the cloth stack. After filling the reservoir with slurry, the pump line was closed and compressed nitrogen gas at ~700 psi was used to force the slurry through the preform and the liquid through the filter. The amount of slurry applied to each panel was calculated beforehand to fill the cloth stack with alumina particles to achieve a green density of 60%. After infiltration, the panels were demolded and placed in plastic bags to dry slowly over the course of several days. After drying the composites were heat treated at 1,000°C for 30 min. Composites were given a final heat-treatment at 1,200°C for 5 h. In addition to the N610/M/A composite panels, control panels containing uncoated fibers were manufactured with the same procedure.

The N610/M/A composite panel had a thickness of 2.4 mm, a density of ~3.18 g/cm^3 and a fiber volume of approximately 33%. The N610/A panel had a thickness of 2.0 mm, a density of ~3.22 g/cm^3 and a fiber volume of approximately 39%. The overall microstructure of the N610/M/A composite is presented in Fig. 1, which shows 0° and 90° fiber tows as well

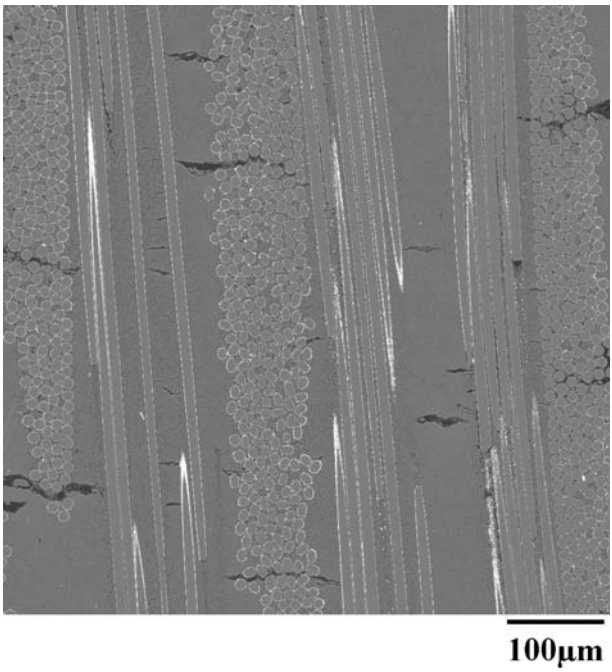

Fig. 1 Micrograph of the as-processed N610/M/A composite showing shrinkage cracks (backscatter SEM image), *bright white* areas are the monazite coating

as shrinkage and sintering cracks that occurred during the cooling stage of the composite processing.

A servocontrolled MTS mechanical testing machine equipped with hydraulic water-cooled wedge grips, a compact two-zone resistance-heated furnace, and two temperature controllers was used in all tests. An MTS TestStar II digital controller was employed for input signal generation and data acquisition. Strain measurement was accomplished with an MTS high-temperature air-cooled uniaxial extensometer of 12.5-mm gage length. Tests in steam environment employed an alumina susceptor (tube with end caps), which fits inside the furnace. The specimen gage section is located inside the susceptor, with the ends of the specimen passing through slots in the susceptor. Steam is introduced into the susceptor (through a feeding tube) in a continuous stream with a slightly positive pressure, expelling the dry air and creating a near 100% steam environment inside the susceptor. For elevated temperature testing, thermocouples were bonded to the specimen using alumina cement (Zircar) to calibrate the furnace on a periodic basis. The furnace controllers (using non-contacting thermocouples exposed to the ambient environment near the test specimen) were adjusted to determine the settings needed to achieve the desired temperature of the test specimen. The determined settings were then used in actual tests. The power settings for testing in steam were determined by placing the specimen instrumented with thermocouples in steam environment and repeating the furnace calibration procedure. Fracture surfaces of failed specimens were examined using SEM (FEI Quanta 200 HV) as well as an optical microscope (Zeiss Discovery V12). The SEM specimens were carbon coated.

All tests were performed at 1,100°C. Dog bone shaped specimens of 152 mm total length with a 10-mm-wide gage section were used in all tests. In all tests, a specimen was heated to test temperature at a rate of 1°C/s, and held at temperature for additional 20 min prior to testing. Tensile tests were performed in stroke control with a constant displacement rate of 0.05 mm/s in laboratory air. Creep-rupture tests were conducted in load control in

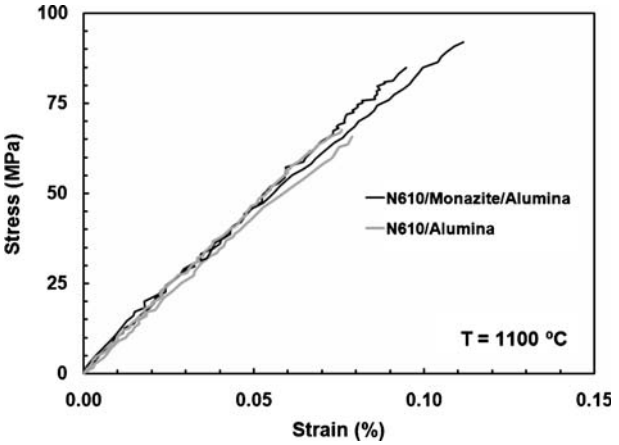

Fig. 2 Tensile stress-strain curves for N610/A and N610/M/A ceramic composites at 1,100°C. All data are adjusted for V_f=0.33

accordance with the procedure in ASTM standard C 1337 in laboratory air and in steam. Specimens were loaded to the creep stress level at the rate of 15 MPa/s. Creep run-out was defined as 100 h at a given creep stress. In each test, stress-strain data were recorded during the loading to the creep stress level and the actual creep period. Thus both total strain and creep strain could be calculated and examined. To determine the retained tensile strength and modulus, specimens that achieved run-out were subjected to tensile test to failure at 1,100°C. It is worthy of note that in all tests reported below, the failure occurred within the gage section of the extensometer. In some cases one specimen was tested per test condition. The authors recognize that this is a limited set of data. However, extreme care was taken in generating the data. Selective duplicate tests have demonstrated the data to be very repeatable. This exploratory effort serves to identify the behavioral trends and to determine whether a more rigorous investigation should be undertaken.

Table 1 Summary of creep-rupture results for N610/A and N610/M/A ceramic composites at 1,100°C in laboratory air and in steam

Test environment	Creep stress (MPa)	Creep strain (%)	Time to rupture (h)
N610/Monazite/Alumina composite			
Air	32	0.07	100[a]
Air	64	0.21	100[a]
Air	72	0.78	100[a]
Steam	32	1.32	51.9
Steam	48	1.92	7.58
Steam	64	1.45	2.37
Steam	72	2.25	2.25
N610 /Alumina composite			
Air	41 (35[b])	0.07	13.5
Air	61 (52[b])	0.08	3.43
Steam	30 (26[b])	0.69	15.8
Steam	41 (35[b])	0.02	0.01

[a] Run-out

[b] Adjusted for V_f=0.33

3 Results and Discussion

3.1 Monotonic Tension

Tensile stress-strain behavior of N610/M/A and N610/A ceramic composites at 1,100°C is typified in Fig. 2. In order to facilitate comparison between results obtained for specimens with different fiber volume fractions, data in Fig. 2 were adjusted for V_f=0.33. It is seen that both materials exhibit typical fiber-dominated composite behavior, all stress-strain curves are nearly linear to failure. For the N610/A composite, the average ultimate tensile strength (UTS) was 66.6 MPa (adjusted for V_f=0.33), the average elastic modulus was 84.1 GPa (adjusted for V_f=0.33), and the average failure strain was 0.08 %. For the N610/M/A composite, the average UTS was 88.5 MPa, the average elastic modulus was 92.2 GPa, and the average failure strain was 0.11 %. The addition of the monazite coating results in ~33% increase in UTS and a 9.6% increase in modulus. However, these improvements in strength and modulus are accompanied by a ~38% increase in failure strain. Note that the beneficial effect of monazite fiber coating on the composite UTS observed here is consistent with that reported in prior work [32].

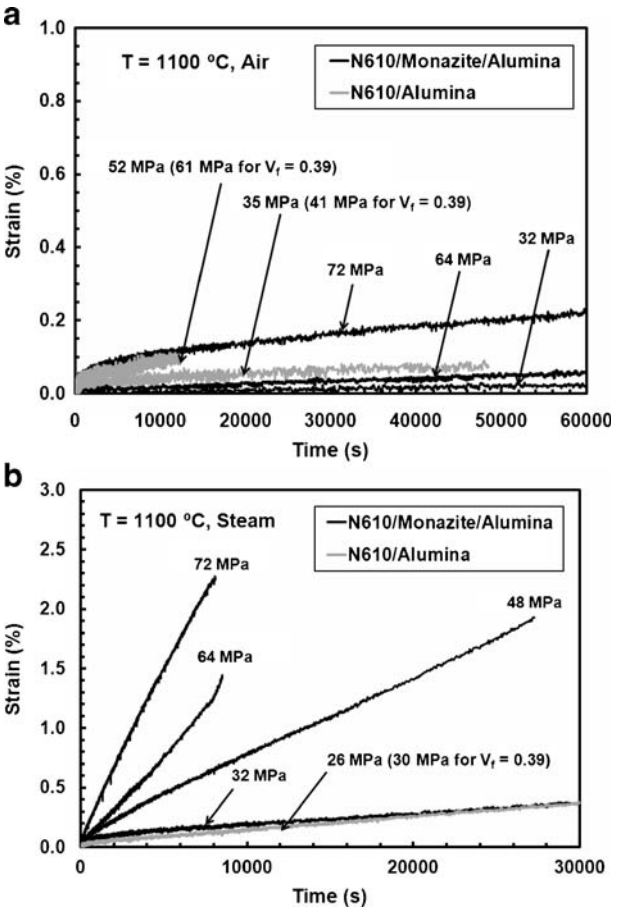

Fig. 3 Creep strain vs time curves for N610/A and N610/M/A ceramic composites at 1,100°C: **a** in air and **b** in steam. All stress levels are adjusted for V_f=0.33

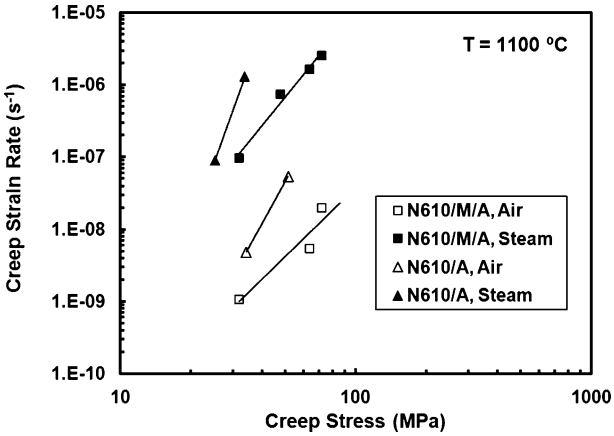

Fig. 4 Minimum creep rate as a function of applied stress for N610/A and N610/M/A ceramic composites at 1,100°C. All data are adjusted for V_f=0.33

3.2 Creep-Rupture

Results of the creep-rupture tests are summarized in Table 1. To facilitate comparison between data obtained for N610/M/A with the fiber volume fraction V_f=0.33 and for N610/A with the V_f = 0.39, all stress levels mentioned in this section are adjusted for V_f=0.33.

Creep strain vs time curves obtained for N610/M/A and N610/A composites at 1,100°C in air and in steam are shown Fig. 3a and b, respectively. The time scale in Fig. 3a and b is reduced in order to clearly show the creep curves produced at higher stress levels. Creep curves produced in all tests conducted in air exhibit primary and secondary creep regimes, but no tertiary creep. Transition from primary to secondary creep occurs early in creep life, secondary creep persists for the remainder of the creep test. All monazite-containing specimens tested in air achieved creep run-out, defined as survival of 100 h at a given creep stress. In the case of the uncoated fiber specimens, the creep run-out was not achieved. For N610/M/A CMC, creep strains accumulated at stress levels ≥64 MPa significantly exceed the failure strain obtained in the tension test. In contrast, creep strains obtained for the N610/A composite are comparable to the failure strain produced in the tension test.

Results in Fig. 3 reveal that test environment has little influence on the appearance of the creep curves obtained for both N610/A and N610/M/A composites. The creep curves produced by each composite in steam are qualitatively similar to the creep curves obtained

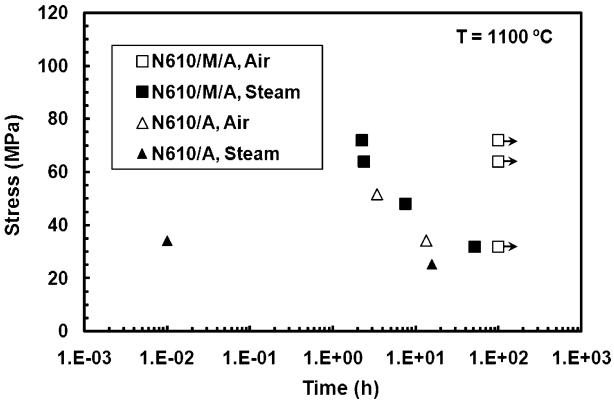

Fig. 5 Creep stress vs time to rupture for N610/A and N610/M/A ceramic composites at 1,100°C. All data are adjusted for V_f=0.33

Table 2 Retained properties of the N610/M/A specimens subjected to prior creep at 1,100°C in air

Creep stress (MPa)	Retained strength (MPa)	Strength retention (%)	Retained modulus (GPa)	Modulus retention (%)	Strain at failure (%)
32	95.8	108	79.4	88	0.13
64	119	134	80.3	87	0.15
72	114	129	70.3	77	0.16

for that material in air, although some tertiary creep is observed at 64 MPa in steam for N610/M/A. However, the presence of steam had a noticeable effect on creep strains and creep lifetimes of both CMCs. Specimens of both composites tested in steam accumulated significantly more creep strain than those tested in air. For N610/A, creep strain produced at 26 MPa in steam was approximately an order of magnitude higher than the creep strains produced in air. For N610/M/A, creep strain accumulated at 32 MPa in steam was nearly 20 times that obtained in air. While the N610/M/A CMC survived 100 h of creep at 72 MPa in air, neither CMC achieved creep run-out in steam.

Minimum creep rate was reached in all tests. Creep rate as a function of applied stress is presented in Fig. 4. It is noteworthy that at 1,100°C in air, the secondary creep rate of the uncoated fiber composite can be as high as ten times that of the monazite containing composite. As expected the minimum creep rates increase with increasing applied stress. In the case of the N610/M/A composite, an increase in creep stress from 32 MPa to 72 MPa causes the creep strain rate to increase by an order of magnitude. For the N610/A composite the same tenfold increase in creep strain rate is caused by an increase in creep stress from 34 MPa to only 52 MPa. The presence of steam accelerates creep rates of both materials. In the case of N610/M/A, creep rate in steam is at least two orders of magnitude higher than that obtained in air for a given stress. The same observation can be made for the N610/A composite. Fitting the experimental data obtained for N610/M/A in air with a temperature-independent Norton-Bailey equation of the form $\dot{\varepsilon} = A\sigma^n$ yields the stress exponent $n \approx 3$, which is close to that reported for the Nextel 610 fibers [33]. Fitting the N610/M/A creep results obtained in steam yields the stress exponent $n \approx 4$. This somewhat higher stress exponent may be due to a contribution from the matrix. Note that a similar value of stress

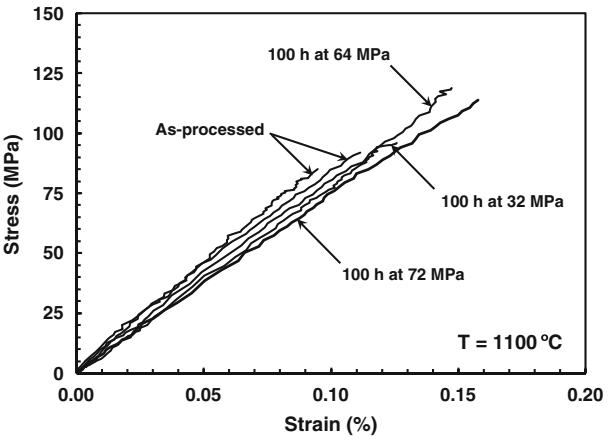

Fig. 6 Effect of prior creep at 1,100°C in air on tensile stress-strain behavior of N610/M/A ceramic composite

exponent ($n \approx 3.5$) was reported in prior work [32] for the N610/M/A composite tested at 1,100°C in air. However, the monazite containing composite examined in this study and the N610/M/A CMC investigated in prior work [32] were fabricated using (i) different fiber architectures, (ii) different methods of applying monazite fiber coating, and (iii) different matrix and composite processing methods. Therefore a direct comparison of the results obtained for these two materials is not possible.

Stress-rupture behavior is summarized in Fig. 5. In air, the creep run-out stress for the monazite-containing composite was 72 MPa. Conversely, N610/A did not achieve run-out at 1,100°C in air. The uncoated fiber composite survived 13.5 h at 35 MPa, and only 3.43 h at 52 MPa. The addition of the monazite coating significantly improved the creep performance at 1,100°C in air. As seen in Fig. 5, the presence of steam dramatically reduced creep lifetimes of both composites. Nonetheless, the beneficial effects of the monazite fiber coating are also evident. For the N610/A CMC, the reduction in creep life due to steam at the applied stress level of 35 MPa was ~99%. Contrastingly, for the N610/M/A CMC the degradation of creep life due to steam at the applied stress of 32 MPa was limited to 48%. A severe (~97%) loss of creep life due to steam was observed at the applied stress levels ≥64 MPa.

Retained strength and modulus of the N610/M/A specimens that achieved a run-out are summarized in Table 2. Tensile stress-strain curves obtained for the specimens subjected to prior creep are presented in Fig. 6 together with the tensile stress-strain curve for the as-processed material. It is seen that prior creep had no qualitative effect on tensile stress-strain behavior. Yet, prior creep appears to have a beneficial effect on tensile strength of the coated fiber composite. The strength of the N610/M/A specimens subjected to 100 h of prior creep in air was 8–30% higher than the average UTS of the untested material. Still, a

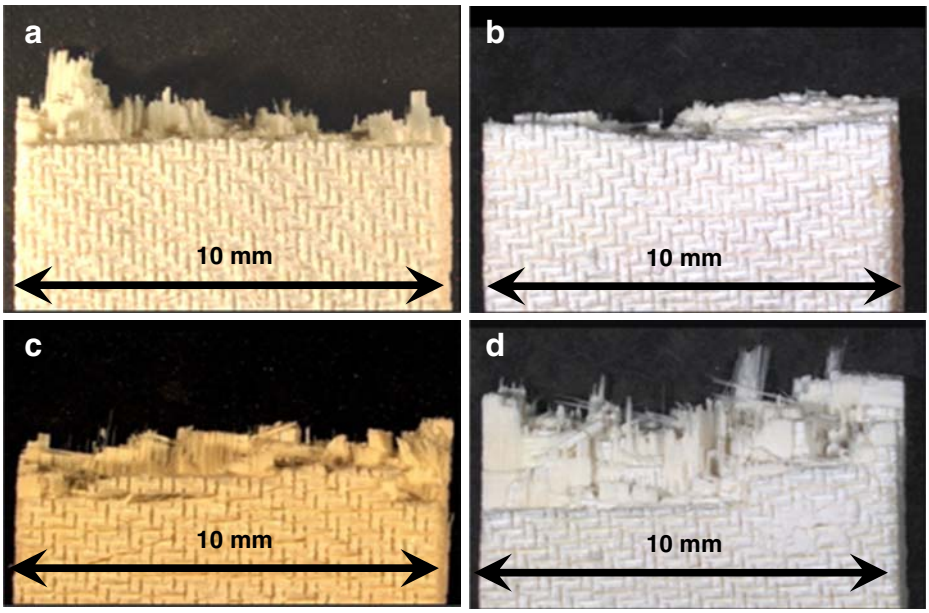

Fig. 7 Optical micrographs of the fracture surfaces of N610/M/A specimens tested at 1,100°C: **a** at 32 MPa in air (t_f>100 h), **b** at 72 MPa in air (t_f>100 h), **c** at 32 MPa in steam (t_f=51.9 h), and **d** at 72 MPa in steam (t_f=2.25 h)

reduction in modulus was observed. The modulus loss due to prior creep was limited to 23%. Prior creep in air also caused a near twofold increase in failure strain, which is consistent with the noticeable increase in strength and decrease in modulus.

3.3 Composite Microstructure

Optical micrographs of the fracture surfaces of the monazite containing specimens are shown in Fig. 7. Surprisingly, although the creep lifetimes in air significantly exceeded those in steam, the fracture surfaces obtained in air and in steam have similar appearance. The fracture surfaces obtained in steam (Fig. 7c and d) exhibit somewhat longer damage zones, but otherwise are akin to those obtained in air (Fig. 7a and b).

Notably, the addition of monazite appears to have little effect on the fracture surface topography of the specimens tested in air. The N610/A fracture surfaces obtained in air (Fig. 8a and b) and those produced in air by the monazite containing specimens (Fig. 7a and b) are alike. Yet the N610/M/A creep lifetimes are strikingly longer than those of the uncoated fiber composite. All N610/M/A specimens achieved a 100-h creep run-out in air, the longest N610/A creep lifetime in air was only 13.5 h. The N610/A fracture surfaces obtained in steam (Fig. 8c and d) exhibit shorter damage zones than the corresponding N610/M/A fracture surfaces (Fig. 7c and d). Still, in steam the N610/M/A creep lifetimes are again markedly longer than those of the N610/A composite.

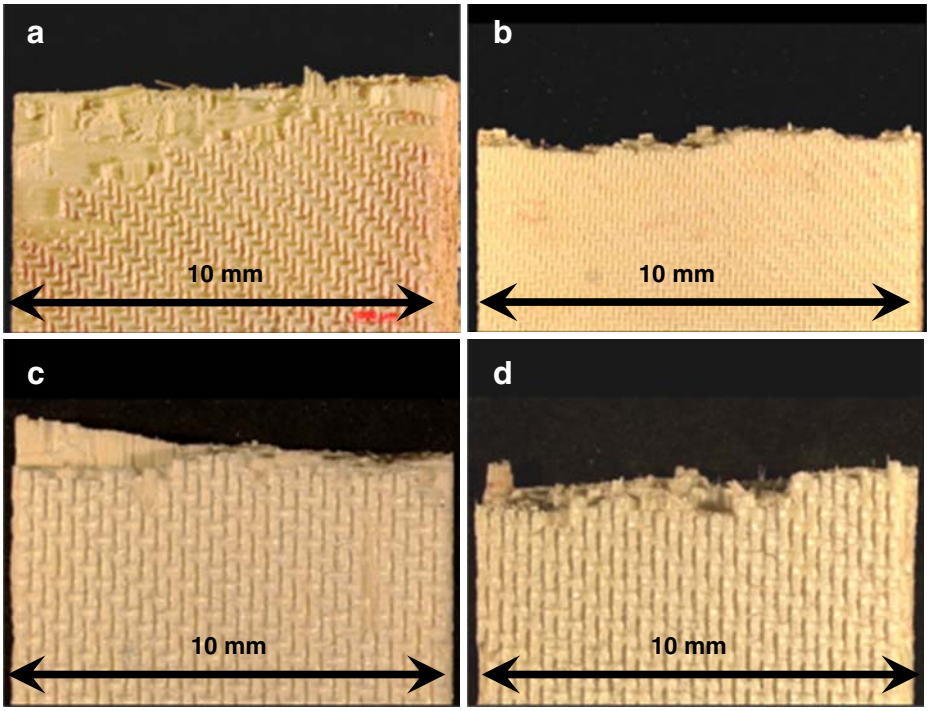

Fig. 8 Optical micrographs of the fracture surfaces of N610/A specimens tested at 1,100°C: **a** at 41 MPa in air (t_f=13.5 h), **b** at 61 MPa in air (t_f=3.43 h), **c** at 30 MPa in steam (t_f=15.8 h), and **d** at 41 MPa in steam (t_f=0.01 h)

The SEM micrographs of the N610/M/A (Fig. 9) and N610/A (Fig. 10) fracture surfaces support the observations given above. All fracture surfaces in Figs. 9 and 10 are dominated by planar regions of coordinated fiber failure. Compare the fracture surface of the N610/M/A specimen tested at 32 MPa in air (Fig. 9a) and that of the N610/A specimen tested at 41 MPa (35 MPa for V_f=0.33) in steam (Fig. 10d). The two fracture surfaces have essentially the same topography. Yet the N610/M/A specimen in Fig. 9a achieved a 100-h creep run-out and failed in a subsequent tensile test, while the N610/A specimen in Fig. 10d failed after mere 36 s of creep. Whereas it was expected that flat areas of brittle-type fracture would dominate the fracture surfaces of the N610/A composite, it was surprising that the fracture surfaces of the monazite containing N610/M/A CMC were likewise predominantly planar. Ongoing research aims to gain a better understanding of the microstructural mechanisms behind the creep performance of both composites.

4 Concluding Remarks

The tensile stress-strain behavior of N610/A and N610/M/A composites was investigated and the tensile properties measured at 1,100°C. The stress-strain behavior of both composites is

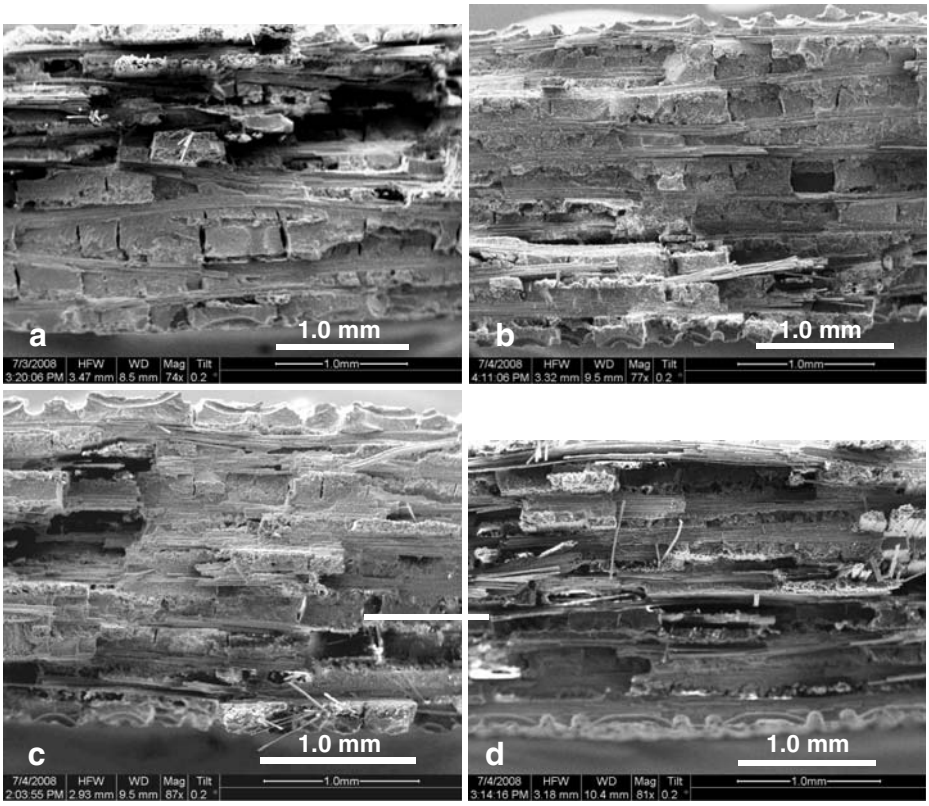

Fig. 9 SEM micrographs of the fracture surfaces of N610/M/A specimens tested at 1,100°C: **a** at 32 MPa in air (t_f>100 h), **b** at 72 MPa in air (t_f>100 h), **c** at 32 MPa in steam (t_f=51.9 h), and **d** at 72 MPa in steam (t_f=2.25 h)

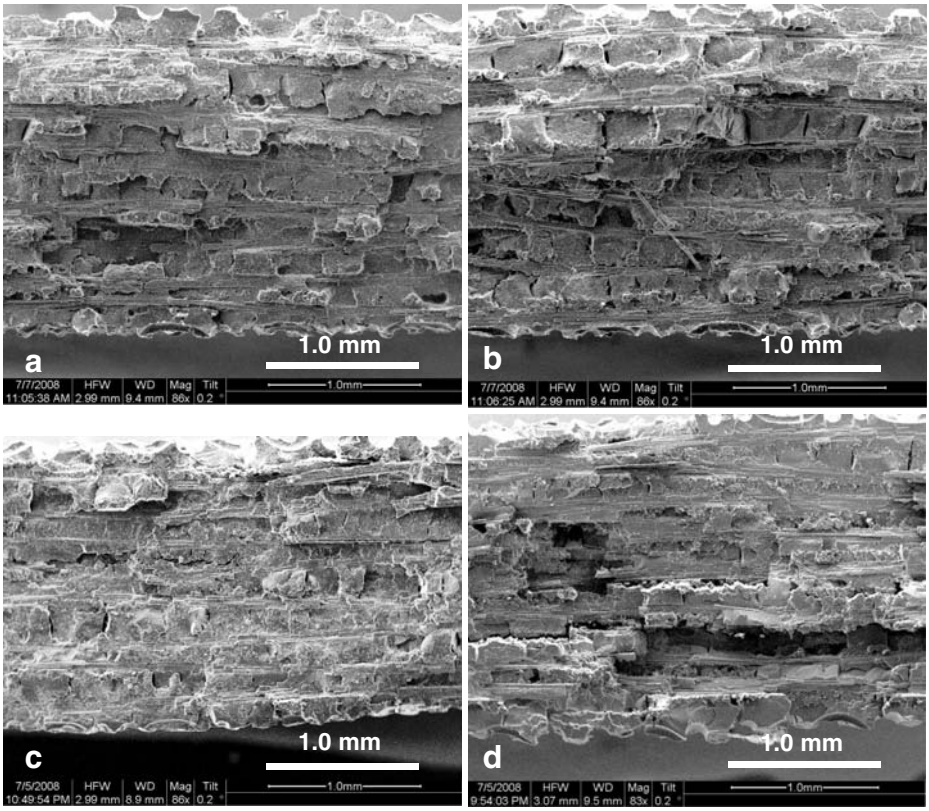

Fig. 10 SEM micrographs of the fracture surfaces of N610/A specimens tested at 1,100°C: **a** at 41 MPa in air (t_f=13.5 h), **b** at 61 MPa in air (t_f=3.43 h), **c** at 30 MPa in steam (t_f=15.8 h), and **d** at 41 MPa in steam (t_f=0.01 h)

nearly linear elastic until failure. The addition of monazite coating results in near 33% improvement in strength and a 9.6% increase in modulus. However, it also causes a ~38% increase in failure strain.

The creep-rupture behaviors of the N610/M/A and N610/A composites were characterized at 1,100°C in air and in steam. Creep test environment has little influence on the appearance of the creep curves of the N610/M/A and N610/A composites. For each composite, the creep curves produced in steam are qualitatively similar to those obtained in air. In contrast, creep strains accumulated by each composite in steam are significantly larger than those produced in air.

Minimum creep rate was reached in all tests. In air, creep strain rates of N610/M/A composite range from 1.1×10^{-9} to 2.0×10^{-8} s^{-1}. In air, the secondary creep rate of N610/A can be an order of magnitude higher than that of the N610/M/A composite. The presence of steam accelerates the creep rates of both composites by at least two orders of magnitude.

For the monazite containing composite the run out stress in air was 72 MPa (81% UTS). The uncoated fiber composite did not achieve run-out in air. The addition of the monazite coating significantly improved the creep performance at 1,100°C in air. Presence of steam dramatically reduced creep lifetimes of both composites. Neither composite achieved run-out in steam. However, the loss of creep resistance due to steam in the case of N610/M/A

was less drastic than in the case of N610/A. At creep stress levels ≤ 35 MPa, the reduction in creep lifetime due to steam was ≈99% for N610/A, but only ≈48% for N610/M/A.

All N610/M/A and N610/A fracture surfaces obtained at 1,100°C are dominated by regions of coordinated fiber failure. The near-planar fracture surfaces suggest the loss of matrix porosity and subsequent matrix densification due to additional sintering.

References

1. Zok, F.: Developments in oxide fiber composites. J. Am. Ceram. Soc. **89**(11), 3309–3332 (2006)
2. Zawada, L.P., Staehler, J., Steel, S.: Consequence of intermittent exposure to moisture and salt fog on the high-temperature fatigue durability of several ceramic-matrix composites. J. Am. Ceram. Soc. **86**(8), 1282–1291 (2003)
3. Schmidt, S., Beyer, S., Knabe, H., Immich, H., Meistring, R., Gessler, A.: Advanced ceramic matrix composite materials for current and future propulsion technology applications. Acta Astronaut **55**, 409–420 (2004)
4. Szweda, A., Millard, M.L., Harrison, M.G.: Fiber-reinforced ceramic-matrix composite member and method for making. U. S. Pat. No. 5 601 674, (1997)
5. Sim, S.M., Kerans, R.J.: Slurry infiltration and 3-D woven composites. Ceram. Eng. Sci. Proc. **13**(9-10), 632–641 (1992)
6. Moore, E.H., Mah, T., Keller, K.A.: 3D Composite fabrication through matrix slurry pressure infiltration. Ceram. Eng. Sci. Proc. **15**(4), 113–120 (1994)
7. Lange, F., Tu, W., Evans, A.: Processing of damage-tolerant, oxidation-resistant ceramic matrix composites by a precursor infiltration and pyrolysis method. Mater. Sci. Eng. A **195**, 145–150 (1995)
8. Mouchon, E., Colomban, P.: Oxide ceramic matrix/oxide fiber woven fabric composites exhibiting dissipative fracture behavior. Composites **26**, 175–182 (1995)
9. Tu, W.C., Lange, F.F., Evans, A.G.: Concept for a damage-tolerant ceramic composite with strong interfaces. J. Am. Ceram. Soc. **79**(2), 417–424 (1996)
10. Evans, A.G., Zok, F.W.: Review: the Physics and mechanics of fiber-reinforced brittle matrix composites. J. Mater. Sci. **29**, 3857–3896 (1994)
11. Kerans, R.J., Parthasarathy, T.A.: Crack deflection in ceramic composites and fiber coating design criteria. Composites A **30**, 521–524 (1999)
12. Kerans, R.J., Hay, R.S., Parthasarathy, T.A., Cinibulk, M.K.: Interface design for oxidation-resistant ceramic composites. J. Am. Ceram. Soc. **85**(11), 2599–2632 (2002)
13. Levi, C.G., Yang, J.Y., Dalgleish, B.J., Zok, F.W., Evans, A.G.: Processing and performance of an all-oxide ceramic composite. J. Am. Ceram. Soc. **81**, 2077–2086 (1998)
14. Mattoni, M., Yang, J., Levi, C., Zok, F.: Effects of matrix porosity on the mechanical properties of a porous matrix, all-oxide ceramic composite. J. Am. Ceram. Soc. **84**(11), 2594–2602 (2003)
15. Zok, F.W., Levi, C.G.: Mechanical properties of porous-matrix ceramic composites. Adv. Eng. Mater. **3**(1–2), 15–23 (2001)
16. Morgan, P.E.D., Marshall, D.B.: Ceramic composites of monazite and alumina. J. Am. Ceram. Soc. **78**(6), 1553–1563 (1995)
17. Morgan, P.E.D., Marshall, D.B.: Functional interfaces for oxide/oxide composites. Mater. Sci. Eng. **A162**, 15–25 (1993)
18. Morgan, P.E.D., Marshall, D.B., Housley, R.M.: High-temperature stability of monazite-alumina composites. Mater. Sci. Eng. **A195**, 215–222 (1995)
19. Chawla, K.K., Liu, H., Janczak-Rusch, J., Sambasivan, S.: Microstructure and properties of monazite ($LaPO_4$) coated saphikon fiber/alumina matrix composites. J. Eur. Cer. Soc **20**, 551–559 (2000)
20. Cazzato, A., Colby, M., Daws, D., Davis, J., Morgan, P., Porter, J., Butner, S., Jurf, R.: Monazite interface coatings in polymer and sol-gel derived ceramic matrix composites. Ceram. Eng. Sci. Proc. **18**(3), 269–278 (1997)
21. Kuo, D.H., Kriven, W.M., Mackin, T.J.: Control of interfacial properties through fiber coatings: monazite coatings in oxide-oxide composites. J. Am. Ceram. Soc. **80**(12), 2987–2996 (1997)
22. Boakye, E.E., Hay, R.S., Petry, M.D.: Continuous coating of oxide fiber tows using liquid precursors: monazite coatings on Nextel 720. J. Am. Ceram. Soc. **82**(9), 2321–2331 (1999)
23. Hay, R.S.: Method for coating continuous tows. U. S. Pat. No. 5 164 229 (1992)
24. Boakye, E.E., Petry, M.D., Hay, R.S., Douglas, L.M.: Monazite coatings on Nextel 720, 610, and Tyranno-SA fiber tows: effects of precursors on fiber strength. Ceram. Eng. Sci. Proc. **21**(4), 229–236 (2000)

25. Fair, G.E., Hay, R.S., Boakye, E.E.: Precipitation coating of monazite on woven ceramic fibers: I. Feasibility. J. Am. Ceram. Soc. **90**(2), 448–455 (2007)
26. Fair, G.E., Hay, R.S., Boakye, E.E.: Precipitation coating of monazite on woven ceramic fibers: II. Effect of processing conditions on coating morphology and strength retention of Nextel™ 610 and 720 fibers. J. Am. Ceram. Soc **91**(5), 1508–1516 (2008)
27. Lee, S.S., Zawada, L.P., Staehler, J., Folsom, C.A.: Mechanical behavior and high-temperature performance of a woven Nicalon™/Si-N-C ceramic-matrix composite. J. Am. Ceram. Soc. **81**(7), 1797–1811 (1998)
28. Zawada, L.P., Hay, R.S., Lee, S.S., Staehler, J.: Characterization and high-temperature mechanical behavior of an oxide/oxide composite. J. Am. Ceram. Soc. **86**(6), 981–990 (2003)
29. Ruggles-Wrenn, M.B., Mall, S., Eber, C.A., Harlan, L.B.: Effects of steam environment on high-temperature mechanical behavior of Nextel™720/alumina (N720/A) continuous fiber ceramic composite. Composites A **37**(11), 2029–2040 (2006)
30. Mehrman, J.M., Ruggles-Wrenn, M.B., Baek, S.S.: Influence of hold times on the elevated-temperature fatigue behavior of an oxide-oxide ceramic composite in air and in steam environment. Comp. Sci. Tech. **67**, 1425–1438 (2007)
31. Keller, K.A., Mah, T.I., Parthasarathy, T.A., Boakye, E.E., Mogilevsky, P., Cinibulk, M.K.: Effectiveness of monazite coatings in oxide/oxide composites after long-term exposure at high temperature. J. Am. Ceram. Soc. **86**(2), 325–332 (2003)
32. Ruggles-Wrenn, M.B., Musil, S.S., Mall, S., Keller, K.A.: Creep Behavior of Nextel™610/ monazite/ alumina composite at elevated temperatures. Comp. Sci. Tech. **66**(13), 2089–2099 (2006)
33. Wilson, D.M., Visser, L.R.: High performance oxide fibers for metal and ceramic composites. Composites: Part A **32**, 1143–1153 (2001)